13

On-chip ATR sensor ($\lambda = 3.4\,\mu$m) based on InAsSbP/InAs double heterostructure for the determination of ethanol concentration in aqueous solutions

© S.A. Karandashev, A.A. Klimov, T.S. Lukhmyrina, B.A. Matveev¶, M.A. Remennyi, A.A. Usikova

Ioffe Institute,
194021 St. Petersburg, Russia

¶ e-mail: bmat@iropt3.ioffe.ru

Received February 7, 2022
Revised April 22, 2022
Accepted April 28, 2022

We discuss photoelectrical properties of an on-chip attenuated total reflection (ATR) sensor for the ethanol concentration measurements in an aqueous solution. The on-chip sensor/microchip was made from a *p*-InAsSbP/*n*-InAs monolithic double heterostructure with three mesas/individual diodes grown on a single n^+-InAs substrate/waveguide. Two heterostructure diodes were used as photodiodes, while the third one - as a LED. The ethanol concentration was measured via an algorithm based on analysis of the I-V characteristic parameters of a photodiode and the L-I characteristics of the LED.

Keywords: photodiodes in the mid-IR range, LEDs in the mid-IR range, on-chip sensor, optical sensors, ATR sensor.

DOI: 10.21883/EOS.2022.08.54772.3236-22

Introduction

Liquid chemical composition sensors using optical methods of measurement have broad medicinal, industrial and indoor applications, because of their dependability and repeatability of the measurement results [1–4]. Utilization of semiconductor technology allowing creation of microsensors, where active elements are integrated into the same monocrystalline chip, contributes into the expansion of their scope of applications (an English term „on-chip sensor", draft translation into Russian — „sistema na kristalle", SNK). In one of the integration options a micro optical pair consisting of optically coupled diode source and radiation receiver with a specific size of active regions from 20 to 300 μm is formed on a common monocrystalline semiconductor substrate [5–8]. Wherein, optical coupling refers to the delivery of light originated from the semiconductor source into the spatially separated radiation receiver [5,6], or the delivery of radiation that do not leave a monolithic chip, i.e. radiation propagating inside transparent substrate [7–9]. In the latter case, a monolithic micro optical pair light-emitting diode (LED)–photodiode (PD) can be used as a sensor of multiply attenuated total reflection (ATR), because the value of photocurrent in PD depends on the refraction index and absorption coefficient of a substance (analyte), which is in optical contact with the substrate. In such a sensor the substrate made of, e.g., InAs, acts as an ATR crystal [7,8]. Application of A^3B^5 semiconductors both as a material for ATR crystal base, and for active elements (i.e., LED and PD) seems to be promising because of several reasons, including no limitations as to using them in the EU, imposed by the RoHS (a Directive on the restriction of using hazardous substances, including Cd and Hg) [10].

One of the benefits of the monolithic embodiment of a on-chip sensor design is the possibility of pro rata decrease of its physical dimensions, because in this case the number of reflections from the ATR/analyte boundary line remains constant, with all other conditions being equal. The useful signal in PD remains constant as well. Reduction of the PD size, and increase of its dynamic resistance, accordingly, is quite relevant for finding a solution that ensures the obtainment of the maximum signal-to-noise ratio when working with modern operational amplifiers of electrical signals [11].

This paper, continuing our studies of the use of monolithic ATR on-chip sensors, demonstrates the perspectives of their application for the ethanol concentration measurements in aqueous solution, which includes calibration algorithm based on the determination of the current-voltage characteristic parameters (I-V characteristics) of active elements of the on-chip sensor based on the double heterostructure (DH) *p*-InAsSbP/*n*-InAs ($\lambda = 3.4\,\mu$m, 300 K) with 4 times reduced area of the active regions of the elements versus samples given in [7,8].

Samples and study methods

The on-chip sensor (Fig. 1) was manufactured from on the InAsSbP/InAs DH; its energy band diagram, as well as the operational capability both of PD, and of LED were earlier described in [12]. The DH layout is given in the inset in the top left corner in Fig. 1, *b*: wide band layer *N*-InAsSbP with the thickness of 3 μm, active layer *n*-InAs with the thickness of 7 μm and the contact layer of *p*-InAsSbP with the thickness of 3 μm were grown on a heavily doped

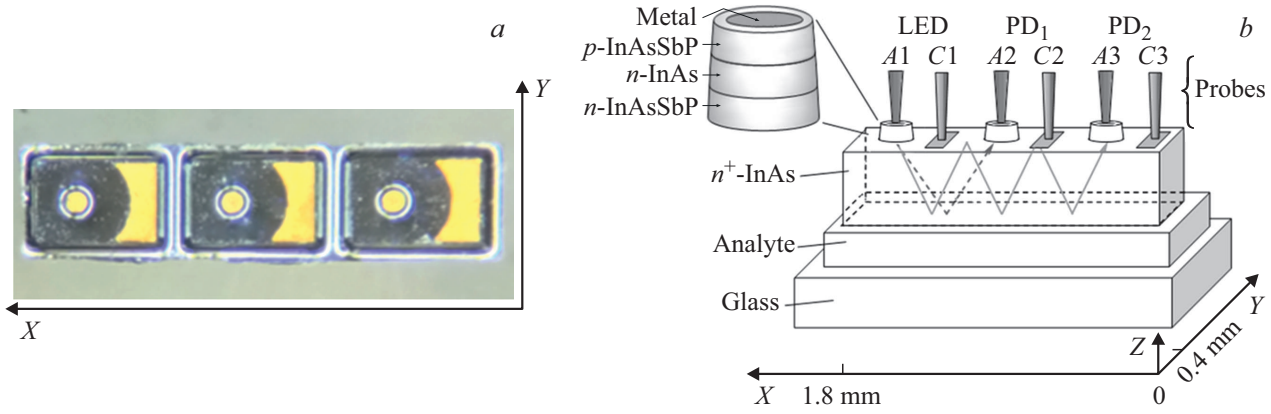

Figure 1. (a) Image of the sensor surface on the terminals side. (b) Sensor schematic. Lines with arrows refer to examples of the beam paths from LED to PD_1 and PD_2. $A1, A2, A3$ — anodes, $C1, C2, C3$ — cathodes. The inset shows DH schematic. Metal — metallic anode, probes — needle probes, analyte — a substance to be analyzed, glass — glass plate.

conductive substrate n^+-InAs, thinned down to $150\,\mu$m, by using the liquid phase epitaxy process.

Diodes were formed by using standard photolithography processes: each diode with the size of 0.4×0.55 mm consisted of round mesa ($Ø_m = 95\,\mu$m) with round metallic anode ($Ø_A = 72\,\mu$m) and metallic cathode located aside of the anode, as shown in Fig. 1. The sensor microchip with the size of 0.4×1.8 mm (see image in Fig. 1, a) consisted of three diodes described above, having a common n-InAs substrate, divided by etching grooves and arranged with the period of $580\,\mu$m (in direction of X in Fig. 1). Long sides of the chip were obtained by the substrate cleaving along the $\{110\}$ planes (directions $\langle 110\rangle$ coincide with the axes X and Y, accordingly, and the direction [001] coincides with the axis Z, as shown in Fig. 1, b). Such samples in the literature also refer to „diode arrays“ [13]; by using this terminology in our paper we dealt with a „monolithic diode array 1×3“.

The diode array was placed onto a polished glass slab („glass“ in Fig. 1) with mechanical locking and electrical connection, provided with gold-plated probes with the tip diameter of $30\,\mu$m, pressed to the contact areas, as shown in Fig. 1, b ($A1-A3$, $C1-C3$). In a series of experiments the layer of liquid (analyte) with the thickness of $1-2\,\mu$m was added between the glass and n^+-InAs substrate. Technical ethanol (96% C_2H_5OH), distilled water and water-alcohol mixture (40% ethanol, 60% distilled water: „Vodka“) were selected as analytes.

The PD I-V characteristics were measured in a CW mode within the range of currents $|I| = 10^{-8}-10^{-4}$ A by means of the SourceMeter Keithley 6430. The derivate of current dependence on voltage near zero bias ($1/R_0$) was obtained by processing the data at $|U| < 10$ mV. The LED I-V characteristics were measured in the pulse-mode ($\tau = 10\,\mu$s, $f = 2$ kHz) within the range $I = 10^{-8}-1$ A. Photocurrent I_{ph} was taken as the difference between the values of the PD current with activated LED and its dark value at $U = 0$. The spectrum of electroluminescence (EL) and current photosensitivity (S_I) of diodes is given in Fig. 2. It also shows the transmittance spectrum of the n^+-InAs substrate; position of its transmittance maximum at the wavelength of $3.4\,\mu$m corresponds to the wavelength of the maximum of production of the spectra of EL and S_I.

The temperature dependence of zero bias resistance (R_0) within the range of 280−340 K was described by standard expression for the current limited by diffusion in InAs diodes:

$$R_0 \sim \exp\left(E_a/(\beta kT)\right), \tag{1}$$

where k is the Boltzmann constant, T is the temperature, $\beta \approx 1$, $E_a = 0.35$ eV.

I-V characteristics at $U_{fb} < 0.35$ V followed the modified Shockley formula:

$$I = I_0\left(\exp\left(\frac{eU}{\beta kT}\right) - 1\right) \tag{2}$$

with the ideality factor $\beta = 1.25$ and the saturation current $I_0 = 4 \cdot 10^{-6}$ A. At high forward bias and pumping currents $I_{fb} = 120-1000$ mA the exponential dependence ($I = I_0 \cdot \exp(eU/\beta kT)$) was changed to linear one ($I_{fb} \sim U_{fb}/R_s$), determined by serial resistance of LED $R_s = 0.27\,\Omega$.

With measurements of the photocurrent the diode № 1 (the leftmost diode in Fig. 1) acted as a LED, the two remaining diodes acted as photodetectors. Measurements of several same-type samples were done, the relationships described below were observed in each of them.

Results and their discussion

Fig. 3 demonstrates I-V characteristics of PD_1 at different LED pumping currents. In both PDs (PD_1 and PD_2) photocurrents (I_{ph}) emergence was detected upon LED activation, wherein the photocurrent in the photodiode, which is closer to LED ($I_{\text{ph}\,1}$), was about ten times higher than in one, which was far from the LED ($I_{\text{ph}\,2}$).

Difference in values $I_{\text{ph}\,1}$ and $I_{\text{ph}\,2}$ is most probably associated both with the difference in optical path from the

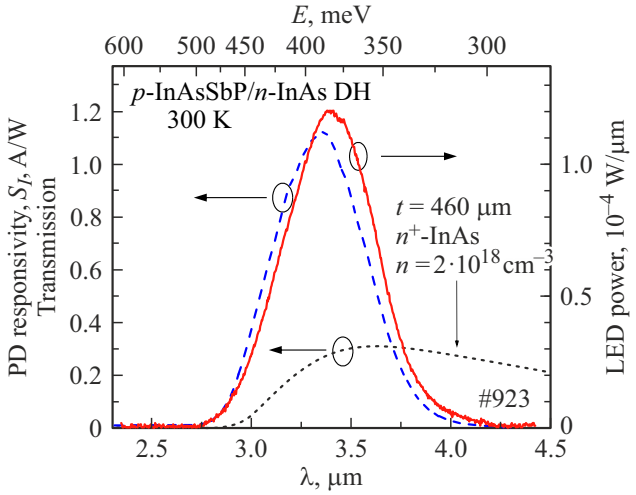

Figure 2. PD sensitivity $U_{PD} = 0$ V (blue dashed curve) and LED EL spectrum at $I_{LED} = 100$ mA (red curve) as a part of the sensor. Optical transmittance of the substrate n^+-InAs with the thickness of 460 μm (black dashed curve).

LED to the PD (Fig. 1) (i.e. contribution of absorbance from the substrate), and with the absorption of the significant portion of radiation from the LED, after reflection from the n^+-InAs/air interface, by the PD_1, which is the nearest to it. As we can see in Fig. 3, *a*, the I-V characteristics of PD_1 at different LED pumping currents intersected at $U_{PD_1} \approx 20$ mV, which was caused by heating of PD_1 as a result of heat released by the operating LED and further transmitted through the substrate to PD_1. The LED current-induced heating affected also the I-V characteristic slope in linear scale, as we can see from data given in Fig. 3, *b*. With the increase of LED current from 0 to 110 mA the PD_1 I-V characteristic slope increased from $9.8 \cdot 10^{-5}\,\Omega^{-1}$ to $1.5 \cdot 10^{-4}\,\Omega^{-1}$, which corresponded to the decrease of the value R_0 from 10200 Ω down to 6630 Ω. A decrease of R_0 in PD_2 also occurred with the increase of the LED current. Subject to expression (1) the specified modifications of R_0 indicated an increase of the temperature of PD_1 by $\Delta T = 8$ K and of PD_2 by $\Delta T = 7$ K with the current of $I_{fb} = 110$ mA flowing in LED. These values of ΔT are comparable with the experimental data in nominally similar structures in [12].

When using the 1×3 diode array as a contact sensor of liquids or solids, the change of its temperature will be caused not only by the current heating of the LED, but also by the temperature and thermal conductivity of the analyte, which may be a source of inaccuracy of the measurements.

In fact, when measuring with the on-chip sensor temperature varying in time, the current transmission coefficient ($CTC = I_{ph}/I_{LED}$), i.e., useful signal from the sensor, due to temperature dependence of the LED power and PD sensitivity, will also vary [4,8,12,14]. In order to eliminate the effect of that dependence for the measurement result, calibration algorithms are usually used that allow to analyze the on-chip sensor CTC obtained at different temperatures.

Within the framework of the calibration algorithm used also in paper [8], the LED current heating effect is used for the on-chip sensor heating in general, which allows for all studied substances to obtain the CTC values at the same temperature T_m, but at different LED pumping currents. Knowing that the PD sensitivity does not depend on the power of radiation falling onto it, we may assume that CTC at T_m depends only on the internal quantum efficiency of LED (IQE), which is more frequently described by the ABC-model [15]:

$$IQE = \frac{Bn_{inj}}{A + Bn_{inj} + Cn_{inj}^2}, \qquad (3)$$

where n_{inj} — concentration of non-equilibrium (injected) charge carriers, A, B, C — experimentally determined coefficients responsible for the Shockley–Read–Hall recombination, radiative and Auger-non-radiative recombination, accordingly. Parameters $A-B-C$ with the selected temperature are fundamental characteristics of the LED, which were studied in many LEDs of visible [14] and middle IR range [16]. Based on the ABC-model, at a constant temperature, the IQE depends only on n_{inj}. Therefore, for the comparison of CTC (I_{ph}/I_{LED}), obtained at T_m, but at different pumping currents in LEDs, the values of CTC (I_{ph}/I_{LED}) must be normalized by the values of CTC ($(I_{ph}/I_{LED})_{ABC}$) of optical pair „LED-external photodetector“ at the LED temperature equal to T_m.

In Fig. 4 black dots connected by dashed line show the dependence of CTC (I_{ph}/I_{LED}) of the pair LED−PD_1 on the current in the LED operated in CW mode, i.e. during heating. Solid line in the same figure shows the dependence of the CTC in non-monolithic („discrete“) optical pair $(I_{ph}/I_{LED})_{ABC}$ on the LED pumping current in pulse mode (10 μs, 2 kHz). A discrete optical pair consisted of spatially separated PDs based on the solid solution of CdHgTe and of LED similar to ones used in the on-chip sensor. The latter one was placed onto a heat sink, i.e., we may consider that the LED was not heated, since along the pulse duration a minor amount of heat was released, which was efficiently removed to the package body and dissipated. For the sake of convenience of further use the dependence $(I_{ph}/I_{LED})_{ABC}$ was normalized so that its value at $I_{LED} = 50$ mA coincided the value of (I_{ph}/I_{LED}) at $I_{LED} = 50$ mA. It is clear that in case of absence of heating the CTC is falling slower, and the CTC dependence on the LED current differs from that obtained in the presence of heating.

Fig. 5 shows the dependence of R_0 in PD_1 on the on-chip sensor CTC. Introduction of a layer of liquid with the thickness of 1−2 μm between the substrate of InAs and the glass resulted in the growth of R_0 (temperature reduction of the $p-n$ junction) due to the sensor cooldown as far as the analyzed liquid is evaporated. It should be noted that the values of R_0 at zero current of the LED also depended on the analyte evaporation rate, so, when ethanol was added the R_0 increased by 1900 Ω, i.e. the sensor cooled down by 3.5 K relative to the indoor ambient temperature.

For the analysis we selected the value $T_m = 299$ K, corresponding to $R_0 = 8400\,\Omega$. At that temperature the

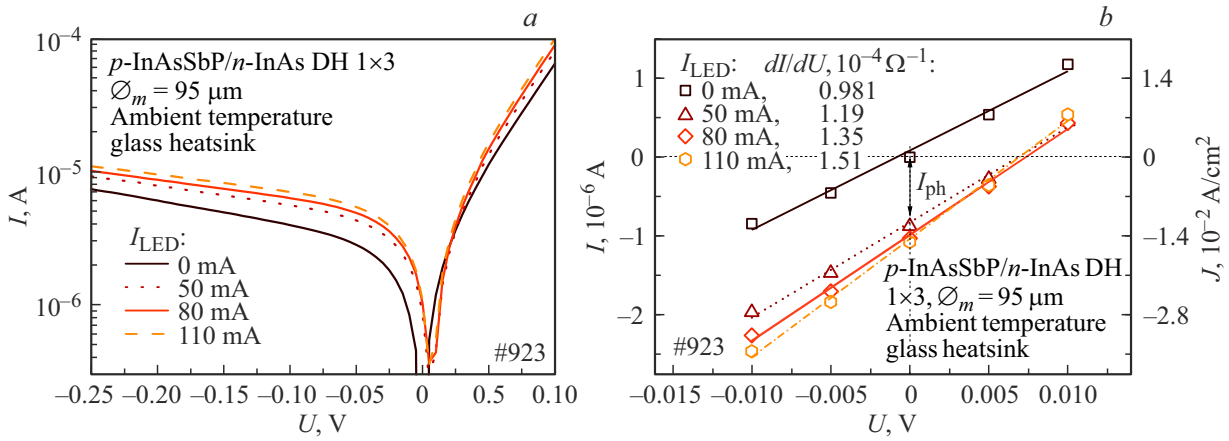

Figure 3. The I-V characteristics of PD_1 (used contacts: $A2$, $C2$) with serial resistance $R_s = 0.27\,\Omega$ in the micro optopair (without analyte), at several LED pumping currents (used contacts: $A1$, $C1$).

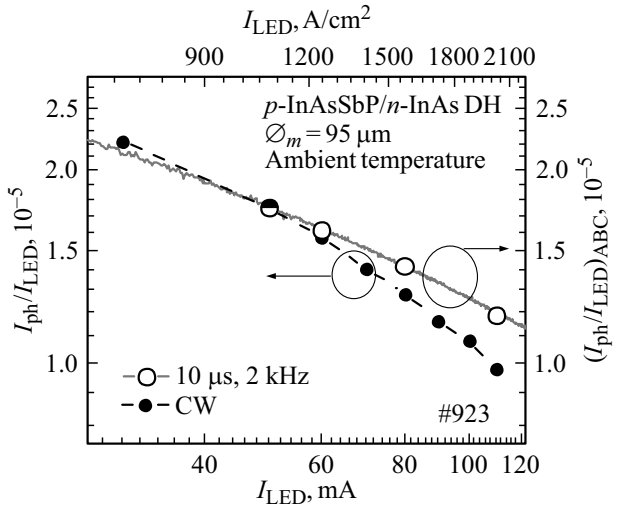

Figure 4. Solid line — dependence of $(I_{ph}/I_{LED})_{ABC}$ on the LED pumping current when working in pulse mode, hollow dots refer to the values used in Table. Dashed line — I_{ph}/I_{LED} of the micro optopair LED–PD_1 on the LED pumping current, solid dots refer to experimental values.

CTC turned to $0.96 \cdot 10^{-5}$, $1.25 \cdot 10^{-5}$, $1.5 \cdot 10^{-5}$ and $1.7 \cdot 10^{-5}$ for ethanol, „Vodka“, water and the case without analyte, accordingly (see Table). These values were obtained at various pumping currents (I_{LED}), and these must be normalized. As calibration curve during normalization it is convenient to use the dependence $(I_{ph}/I_{LED})_{ABC}$, obtained at $T_m = 299$ K, however, herein we decided to use the data (Fig. 4, $(I_{ph}/I_{LED})_{ABC}$), obtained at the indoor ambient temperature. It is permissible, because in Fig. 5 the values are considered at the temperature exceeding the indoor ambient temperature only by 4 K.

Table shows the LED pumping current (I_{LED}) at which the CTC values were obtained, and the density of that current (J_{LED}), which is understood as the LED pumping current ratio to the mesa area. The same Table gives the CTC values obtained in the pulse mode ($(I_{ph}/I_{LED})_{ABC}$, Fig. 4, hollow dots), and the CTC values obtained with different analytes (I_{ph}/I_{LED}, Fig. 5). The latter two values were used for the described normalization process. The values obtained as a result of normalization indicate the transparency of the optical path of LED–PD_1 (normalized transparency of the optical system). The change of transparency in case of the analyte change related both with the change of the critical angle, and with the evanecsent wave absorption at the InAs/analyte interface. According to Table, the normalized transparency of the optical system is gradually rising as far as the ethanol concentration is decreased. As seen from the Table, the transparency value for the case of „Vodka“ is close to the sum of values for pure ethanol and water with the coefficients equal to the alcohol content in the solution.

The paper [8] dealt with a similar measurement of the normalized transparency of the optical system in the

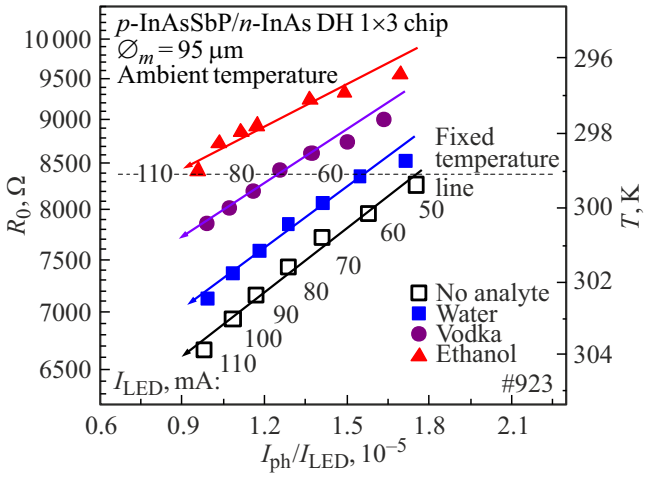

Figure 5. Dependence of the resistance of PD_1 at zero bias on the CTC of the sensor when using different analytes. Arrows refer to track lines of the data sets and directions of LED current value increase.

Table. The values used for calibration procedure, and normalized transparency of the optical system, as a result

1	2	3	4	5	6	7	8	9
Conditions		InAs/air	InAs/liquid				InAs/liquid	
I_{LED}, mA	$J_{LED} \times 10^{-3}$, A/cm^2	$(I_{ph}/I_{LED})_{ABC} \times 10^3$ (Fig. 4)	Analyte	Ethanol, %	$I_{ph}/I_{LED} \times 10^5$ (Fig. 5)	Transparency col(6)/col(3)	$J_{LED} \times 10^{-3}$, A/cm^2 in [8]	Transparency in [8]
110	1.94	1.18	Alcohol	96	0.98	0.83	0.45	0.70
80	1.41	1.41	„Vodka“	40	1.28	0.91	0.45	0.82
60	1.06	1.61	Water	0	1.57	0.98	0.26	0.88
InAs/air							InAs/air	
50	0.88	1.75	No analyte	–	1.75	1.0	–	–

sensor with the two times higher mesa diameter than it is herein. Such a difference results in that the values of the LED current, similar to those in paper [8], herein correspond to several times higher LED current density, as shown in Table. In other words, herein for the calibration procedure we used the dependence area $(I_{ph}/I_{LED})_{ABC}$ with higher concentration of injected carriers and lower quantum efficiency. Regardless of the use of a calibration method, which is a bit different from the optimum one, as well as a reduced area of the active elements, versus paper [8], relative changes of the normalized transparencies for each analyte obtained herein are close to those obtained in our previous article [8], as shown in Fig. 6.

According to the comparison of data hereof and the data in [8], given in Table, double decrease of the active elements mesa diameter resulted in four-time increase of dynamic resistance at the zero bias R_0. On the other hand, the sensor CTC at comparable LED pumping level is only $\sim 25\%$ of that declared earlier [8]; it is quite clear, subject to a small area of the radiation collection, which is $\sim 25\%$ of the used earlier. This disadvantage can easily be eliminated, by increasing the ratio of PD area to the LED area, which is planned to be done at the nearest future.

The electrical measurement protocol used herein is not the optimum one: measurement of the photocurrent I_{ph} and dynamic resistance at the zero bias R_0 in the same PD complicates the circuit engineering when designing the liquid analyzer. Division of the PD_1 and PD_2 functions, namely the use of the PD_1 for the photocurrent measurement, and the PD_2 — for the sensor temperature control is promising in that context.

It should be noted that the waveguide material used in our ATR sensor — InAs — has a high refraction index ($\check{n} = 3.4$), which allows to measure a wide class of substances, for example, polymers ($\check{n} = 1.4-1.6$).

Conclusion

Therefore, the paper demonstrated that the photocurrent in an activated monolithic LED-photodiode on-chip pair based on the *p*-InAsSbP/*n*-InAs double heterostructure with several mesas/diodes with the diameter of 0.1 mm, formed on a common transparent substrate n^+-InAs, depends on the liquid composition having contact to the surface n^+-InAs. Such on-chip optopair, subject to its preliminary calibration (measurement of the current transmission coefficient at different temperature values and the LED pumping currents) can be used as the ATR sensor for the determination of the chemical composition of liquids. The use of the values of

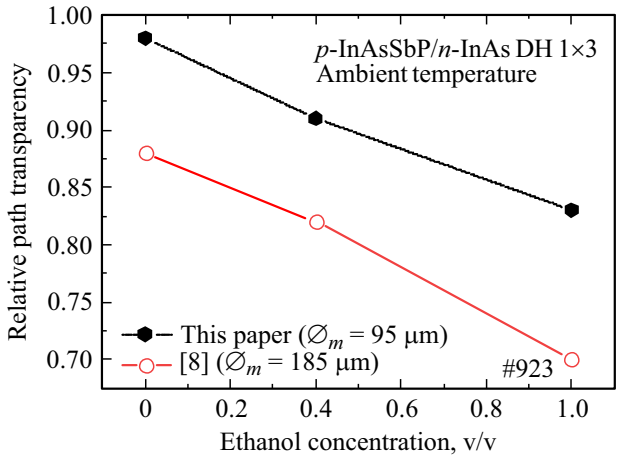

Figure 6. Relative path transparency for 2 optical systems (1×3) at the wavelength of $\lambda = 3.4\,\mu$m, obtained in this paper and in paper [8], depending on the volume fraction of ethanol in the aqueous solution.

Figure 7. Logo of the project „*Embedded Electronic solutions for Polymer Innovative Scanning Methods using Light Emitting devices for diagnostic Routines*“ #945320.

dynamic resistance at the zero bias (R_0) and photocurrent of the photodiode (I_{ph}), as well as the data obtained from preliminary calibration, allow to measure solved substance concentration, for example, to evaluate alcohol content in the water-alcohol solution, which enables to create ultra-small alcoholmeters in the future. The approaches and algorithms obtained in the paper can be useful also for the creation of sensors for the study of solid bodies, e.g., polymers.

Acknowledgments

The authors thank N.D. Il'inskaya, A.A. Lavrov, as well as the personnel of IoffeLED Ltd. for the assistance provided during the studies.

Funding

A part of the paper performed at Ioffe Institute, was initiated by the start of joint studies under the project El Peacetolero (#945320) within the framework of the EU program HORIZON-2020 (Fig. 7) and was funded with support from the Ministry of Science and Higher Education of the Russian Federation for the implementation of the project „Embedded Electronic solutions for Polymer Innovative Scanning Methods using Light Emitting devices for diagnostic Routines" (№ RF 225121X0001, agreement № 075-15-2021-936).

Conflict of interest

The authors declare that they have no conflict of interest.

References

[1] J. Hodgkinson, R.P. Tatam. Meas. Sci. Technol., **24** (1), 012004 (2012). DOI: 10.1088/0957-0233/24/1/012004
[2] F. Seichter, J. Vogt, E. Tütüncü, L.T. Hagemann, U. Wachter, M. Gröger, S. Kress, P. Radermacher, B. Mizaikoff. J. Breath Res., **15** (2), 026013 (2021). DOI: 10.1088/1752-7163/ab8dcd/
[3] C.S. Huertas, O. Calvo-Lozano, A. Mitchell, L.M. Lechuga. Front. Chem., **7**, 724 (2019). DOI: 10.3389/fchem.2019.00724
[4] B.A. Matveev, G.Yu. Sotnikova. Opt. Spectrosc, **127** (2), 322 (2019). DOI: 10.1134/S0030400X19080198.
[5] V.N. Tarasov. RF Patent № RU 2112228 C1, (1998) (in Russian).
[6] N.V. Kryzhanovskaya, E.I. Moiseev, A.M. Nadtochiy, A.M. Kharchenko, M.M. Kulagina, S.A. Mintairov, N.A. Kalyuzhny, M.V. Maksimov, A.E. Zhukov. Pis'ma v ZhTF **46** (13), (2020) (in Russian) DOI: 10.21883/PJTF.2020.13.49582.18301
[7] S.A. Karandashev, T.S. Lukhmyrina, B.A. Matveev, M.A. Remennyi, A.A. Usikova. Opt. Spectrosc., **129** (9), 1333 (2021). DOI: 10.1134/S0030400X21090101.
[8] S.A. Karandashev, T.S. Lukhmyrina, B.A. Matveev, M.A. Remennyi, A.A. Usikova. Phys. Status Sol. (a), **219** (2), 2100456 (2022). DOI: 10.1002/pssa.202100456
[9] L. Chen, X. An, J. Jing, H. Jin, Z. Chu, K.H. Li. ACS Appl. Materials & Interfaces, **12** (44), 49748 (2020). DOI: 10.1021/acsami.0c13144
[10] Directive 2011/65/EU of the European Parliament and of the Council of 8 June 2011 on the restriction of the use of certain hazardous substances in electrical and electronic equipment. Text with EEA relevance.
[11] G.A. Gavrilov, B.A. Matveev, G.Yu. Sotnikova. Tech. Phys. Lett., **37** (9), 866 (2011). DOI: 10.1134/S1063785011090197.
[12] S.A. Karandashev, B.A. Matveev, M.A. Remennyi, Semiconductors, **53** (2), 139 (2019). DOI: 10.1134/S1063782619020131.
[13] I.C. Sandall, S. Zhang, C.H. Tan. Opt. Express, **21** (22), 25780 (2013). DOI: 10.1364/OE.21.025780
[14] X. Jia, J. Roels, R. Baets, G. Roelkens. Sensors, **21** (16), 5347 (2021). DOI: 10.3390/s21165347
[15] S. Karpov. Opt. Quantum Electron., **47** (6),1293 (2015). DOI: 10.1007/s11082-014-0042-9
[16] A. Krier, E. Repiso, F. Al-Saymari, P. Carrington, A. Marshall, L. Qi, S. Krier, K. Lulla, M. Steer, C. Mac Gregor et al. *Mid-Infrared Optoelectronics* (Elsevier, 2020), p. 59−90. DOI: 10.1016/B978-0-08-102709-7.00002-4